ADVANCED MATERIALS
www.advmat.de

Materials Views
www.MaterialsViews.com

COMMUNICATION

The In-Gap Electronic State Spectrum of Methylammonium Lead Iodide Single-Crystal Perovskites

*Valerio Adinolfi, Mingjian Yuan, Riccardo Comin, Emmanuel S. Thibau, Dong Shi, Makhsud I. Saidaminov, Pongsakorn Kanjanaboos, Damir Kopilovic, Sjoerd Hoogland, Zheng-Hong Lu, Osman M. Bakr, and Edward H. Sargent**

Perovskite semiconductors are one of the most striking advances in the field of thin-film optoelectronic technologies, in particular for photovoltaic applications.[1–4] In recent years, progress in perovskite materials processing has enabled rapid advances in the power conversion efficiency of perovskite-based solar cells beyond the 20% milestone.[5,6] Impressively, this high efficiency comes in tandem with facile, inexpensive fabrication, since these materials can be solution-processed at room temperature on large-area substrates. Among perovskite materials, methylammonium lead iodide ($MAPbI_3$, MA = $CH_3NH_3^+$) stands out as particularly promising for photovoltaics.[7] The need to improve device performance further has spurred many researchers to investigate the fundamental properties of $MAPbI_3$. This semiconductor is usually synthesized in a variety of nanocrystalline forms, and its intrinsic material properties are expected to be significantly modified by extrinsic contributions from the manufacturing process, such as the effects of grain boundaries. This has driven many to investigate the electronic properties of $MAPbI_3$ using simulations. Density functional theory (DFT) has been widely employed to predict and evaluate critical quantities such as the effective mass for holes and electrons that give important information about the charge carrier mobility as well as the energetics of trap states.[8–11] The number of available theoretical studies is substantial, and will benefit from direct experimental validation.

Recently, high-quality $MAPbI_3$ single crystals with sizes of few millimeters were synthesized; [12] an initial characterization revealed an ultra-low density of trap states and of free carriers. Here, we use these macroscopic crystals to obtain an in-depth characterization of the electronic and in-gap properties of $MAPbI_3$. We start with a compositional and optical investigation that confirms the quality of the material. We then experimentally determine the band diagram of the semiconductor with particular attention to its surface properties, fundamental for the applications. The mobility and diffusion length of both electrons and holes are directly measured, as well as the concentration and type of the charge carriers. We determine the density of trap states within the electronic bandgap, identifying defect states close to both the valence and the conduction bands. This ensemble of measurements provides a more complete picture of the electronic properties of $MAPbI_3$. In particular, the study of the surface properties and the trap state spectrum are important for the development of solar cells and the design of light emitting diodes and light detectors.

We synthesized $MAPbI_3$ single crystals using the antisolvent vapor-assisted crystallization technique.[13] As shown in **Figure 1**a, we prepare a solution with the precursors (MAI and PbI_2) in a small crystallizing dish. We cover the dish with aluminum foil and deposit it within a bigger container in which the antisolvent liquid resides. After we seal the outer dish, crystallization begins, with the antisolvent vapor mixing into the inner solution after it flows through an millimeter-sized aperture in the aluminum foil of the small crystallizing dish. The mixture between the solvent and the antisolvent sets the supersaturation conditions that promote the formation of crystalline seeds, which successively grow to the desired size.

To investigate on the purity of the crystals, we first measured the absorbance. As shown in Figure 1b a steep absorption edge is located at ≈810 nm, the characteristic absorption onset wavelength of $MAPbI_3$ single crystals.[14–16] We further analyzed this curve to extract the optical bandgap, found to be 1.52 eV (see Figure S1 in the Supporting Information). To confirm further the quality of our material we performed X-ray diffraction (XRD) measurements on powders ground from single crystals. We obtained XRD with sharp Bragg reflection from tetragonal $MAPbI_3$, shown in Figure 1c, again confirming the purity of our perovskite crystals.

We therefore proceeded to the electronic characterization of the crystals. We sought to investigate, in particular, the surface properties of the crystals. To obtain the position of the valence band of $MAPbI_3$ relative to the vacuum level, we used X-ray photoelectron spectroscopy (XPS) (see Figure S2 in the Supporting Information) and ultraviolet photoemission spectroscopy (UPS)

V. Adinolfi, Dr. M. Yuan, Dr. R. Comin, Prof. P. Kanjanaboos,[+] D. Kopilovic, Dr. S. Hoogland, Prof. E. H. Sargent
Department of Electrical and Computer Engineering
University of Toronto
10 King's College Road, Toronto, Ontario M5S 3G4, Canada
E-mail: ted.sargent@utoronto.ca
E. S. Thibau, Prof. Z.-H. Lu
Department of Materials Science and Engineering
University of Toronto
184 College Street, Toronto, Ontario M5S 3E4, Canada
Dr. D. Shi, Dr. M. I. Saidaminov, Prof. O. M. Bakr
Division of Physical Sciences and Engineering
Solar and Photovoltaics Engineering Center
King Abdullah University of Science and Technology (KAUST)
Thuwal 23955-6900, Saudi Arabia
[+]Present address: Department of Material Science and Engineering, Mahidol University, Bangkok, 10400, Thailand

DOI: 10.1002/adma.201505162

© 2016 WILEY-VCH Verlag GmbH & Co. KGaA, Weinheim

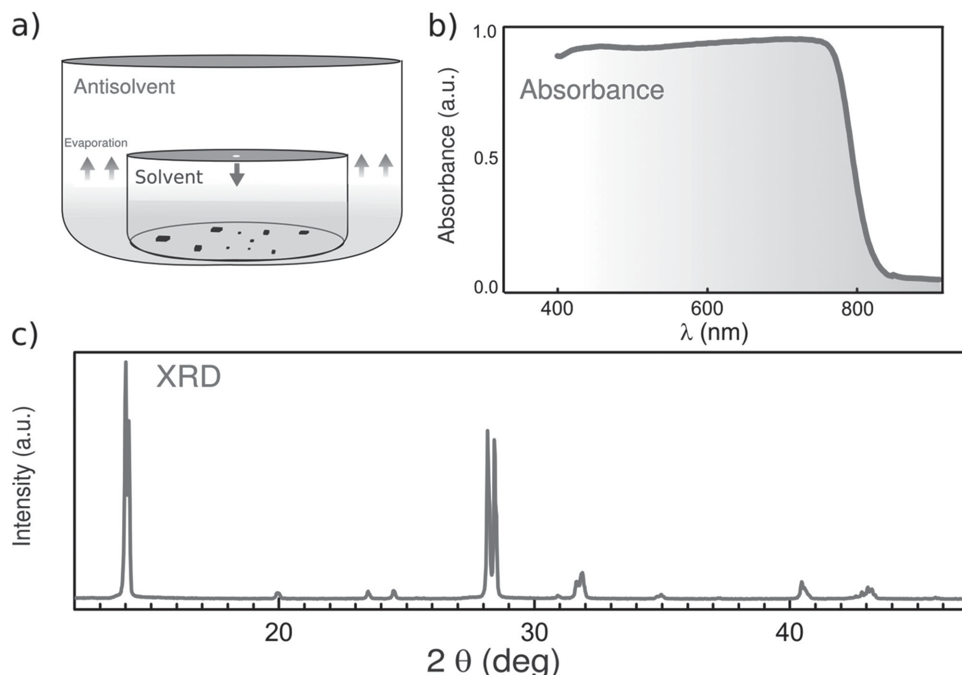

Figure 1. a) Antisolvent vapor-assisted crystallization. b) Absorbance spectrum for $MAPbI_3$ single crystals. c) X-ray diffraction spectroscopy diagram for $MAPbI_3$ single-crystals powder.

(**Figure 2**a).[17–21] Knowing the value of the bandgap, from absorption, we depict the band diagram of the $MAPbI_3$ single crystals (Figure 2c). The ionization potential is IP = 5.7 eV and the inferred electron affinity is χ = 4.18 eV. The Fermi level at the interface is determined, using the Kelvin probe (KP) technique, to lie at 0.12 eV from the conduction band. This measurement indicates a shift of the Fermi level at the crystal surface compared to that in the bulk. The Femi level is shifted at the surface whereas the crystal is close to an intrinsic semiconductor in the bulk.[12,16] This shift can be attributed to the effect of trap states present on the surface of the crystals; these states have been previously identified as the cause for a fast component in the photoluminescence decay trace of $MAPbI_3$[12] single crystals, and have recently been exploited to produce narrowband light detectors.[22] The techniques used for this characterization are surface sensitive, for this reason the surface of the crystals has been accurately cleaned using appropriate wet etching right before the measurements.

To extract the relevant parameters governing electrical transport in the crystal, we performed four-point and Hall effect measurements. Using this technique we found the free carrier concentration to be $n_f \approx 4 \times 10^9$ cm^{-3}, in good agreement with previous reports of a near-intrinsic semiconductor.[12] The Hall coefficient reveals that the majority carriers are electrons with a

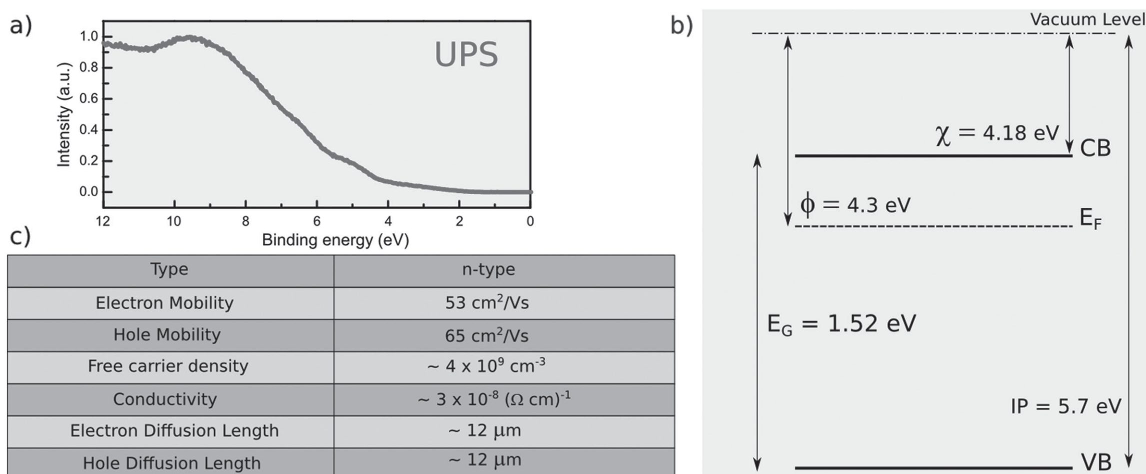

Type	n-type
Electron Mobility	53 cm^2/Vs
Hole Mobility	65 cm^2/Vs
Free carrier density	~ 4 x 10^9 cm^{-3}
Conductivity	~ 3 x 10^{-8} $(\Omega\ cm)^{-1}$
Electron Diffusion Length	~ 12 µm
Hole Diffusion Length	~ 12 µm

Figure 2. a) Ultraviolet photoemission spectroscopy diagram for $MAPbI_3$ near its surface. b) Band diagram for the near-surface of $MAPbI_3$ single crystals drawn according to UPS, XPS, and KP measurements. c) Electronic properties of $MAPbI_3$ single crystals.

 © 2016 WILEY-VCH Verlag GmbH & Co. KGaA, Weinheim

mobility of $\mu_e \approx 50$ cm^2 V^{-1} s^{-1}. Combining these two quantities, the conductivity was estimated to be $\sigma \approx 3 \times 10^{-8}$ Ω^{-1}, again in good agreement with previous findings.[12]

The hole mobility was measured using the space charge limited current (SCLC) technique by fitting the current–voltage characteristic of the crystal in the trap free regime (Child region,[23,24] details in Figure S3, Supporting Information). We obtained a hole mobility of $\mu_h \approx 65$ cm^2 V^{-1} s^{-1}. The electron and hole mobilities are comparable, consistent with previous DFT studies that found comparable effective mass as for electrons and holes.[8] Compared to previous reports[12] we obtained a higher hole mobility, potentially attributable to improvements in sample preparation (see Experimental Section).

Using the Einstein relation to extract the value of the diffusivity $D = \mu k_B T/q$, where k_B is the Boltzmann constant and q the elemental charge, and combining this quantity with the carrier lifetime τ,[12] (estimated from the longer component of the photoluminescence decay) we evaluate the charge carrier diffusion $L_{diff} = (D\tau)^{1/2}$ to be $L_e = L_h \approx 12$ µm. The results of the electronic characterization are summarized in Figure 2c. These numbers reveal the potential of $MAPbI_3$ single crystals for optoelectronic applications, and agree well with the success of nanocrystalline thin-film perovskite solar cells, since long diffusion lengths and low free-carrier concentrations enable high-efficiency photovoltaics. The first quantity allows for efficient extraction of photogenerated carriers over a thickness sufficient to absorb above-bandgap solar radiation; the second property further favors the collection of charge by allowing the presence of an extracting built-in electric field within the active material.

The high diffusion length and the low free-carrier concentration are consequences of an extremely low density of trap states. Defects play a crucial role in the operation of solar cells and light-emitting devices, as they affect the efficiency, the spectral behavior, and the operation as a function of light and electrical biases.[25,26] Knowing the density of in-gap trap states would reveal the position in energy of these defects.[27]

Knowing the effectiveness of the SCLC technique to study electronic properties of trihalide perovskite single crystals, we took the view that the refinement of this approach would enable the mapping of the trap sites within the bandgap. Several studies have been conducted in the past that show how to extract the density of trap states (DOS$_T$) from the temperature dependence of the SCLC current–voltage characteristic in a semiconductor.[28–30] This technique has been employed to investigate organic crystals.[24,31,32] We explain this approach in **Figure 3**. To probe trap states close to both valence and conduction band, we needed to prepare both hole-injecting and electron-injecting devices, respectively, since SCLC exploits

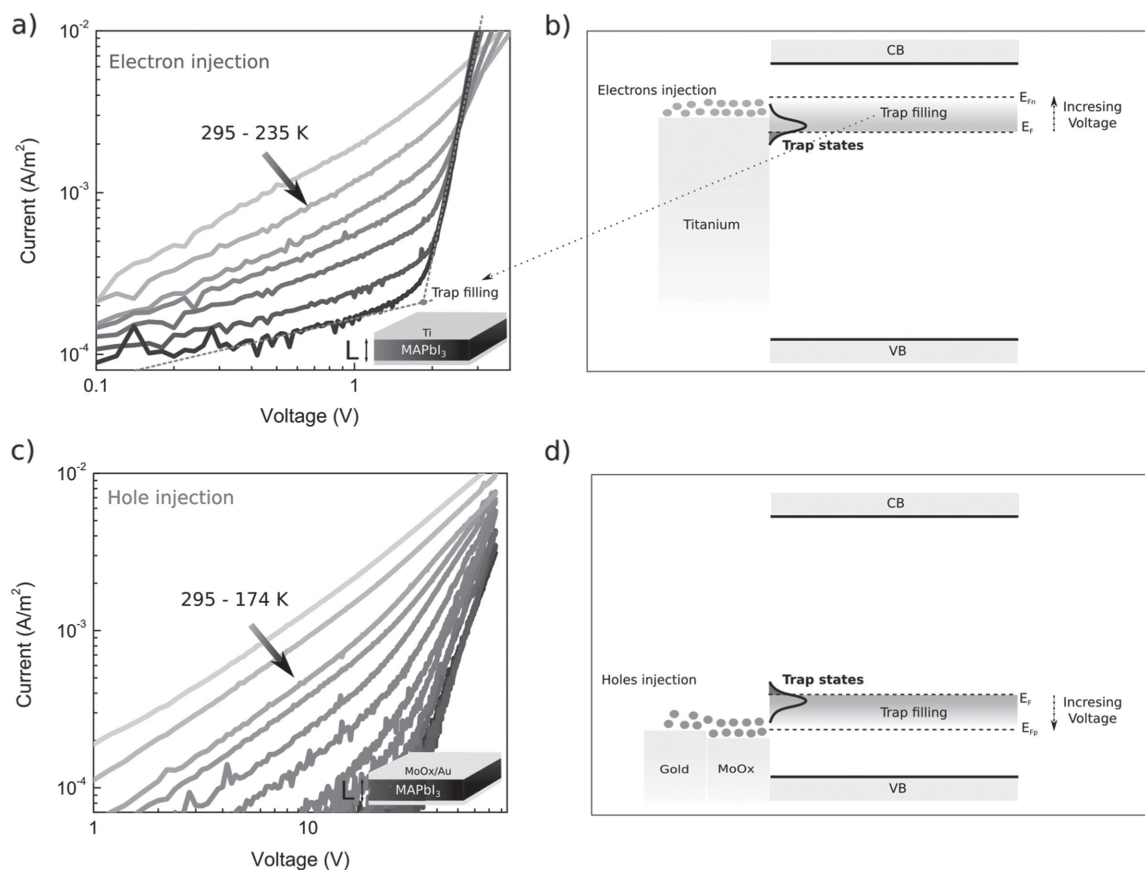

Figure 3. a) I–V curve as a function of temperature for a $MAPbI_3$ single crystal (area × L = (2.7 × 2.3) × 2.0 mm) contacted using titanium (inset) to favor electron injection. b) Scheme illustrating the principles governing the SCLC method in the case of electrons injection. c) I–V curve as a function of temperature for a $MAPbI_3$ single crystal (area × L = (4.0 × 3.7) × 1.3 mm) contacted using MoO_3/Au/Ag (inset) to favor hole injection. d) Scheme illustrating the principles governing the SCLC method in the case of hole injection.

© 2016 WILEY-VCH Verlag GmbH & Co. KGaA, Weinheim

unipolar transport. Hole-injecting devices were realized using MoO_3/Au/Ag contacts, leveraging the deep work function of molybdenum trioxide (MoO_3).[33,34] Electron-injecting devices were fabricated using titanium (Ti), a shallow-work-function metal. The current–voltage characteristics are shown as a function of temperature for both types of devices in Figure 3a,c. We discuss in detail the case of electron-injecting devices (Figure 3b); these considerations apply symmetrically for hole-injecting devices (Figure 3d).

Titanium forms an ohmic contact with the crystals (more details are provided in Figure S5, Supporting Information) and selectively favors electrons injection. At low applied biases the current–voltage is linear. At higher applied bias, the electron transit time becomes comparable with the relaxation time of the semiconductor. In this regime the semiconductor is replenished with electrons; and this excess of charge determines a shift of the Fermi level toward the conduction band. If trap states are present close to the Fermi level, these will be rapidly occupied by the injected electrons, leading to a transition of the current–voltage curve onto a superlinear regime ($I \propto V^m$, $m > 2$), starting at a characteristic voltage $V = V_{TFL}$. This is the trap-filling regime. From the position of V_{TFL}, the temperature, and the derivative $\frac{\partial \ln J}{\partial \ln V}$, reconstruction of the DOS_T is possible.[28]

The equations used in the model are the Ohm's law $J = e\mu n_f(x)F(x)$ and the Poisson equation $\frac{dF}{dx} = -\frac{en_s}{\epsilon}$ where $F(x)$ is the electric field as a function of the spatial coordinate x, J is the current density, ϵ is the dielectric constant, μ the mobility, n_f is the density of free carriers, and n_s is the total density of carriers, both free and trapped. The latter is expressed as $n_s = \int^{E} h(E) f(E, E_F, T)$ where $h(E)$ is the density of trap states within the bandgap, $f(E, E_F, T)$ is the Fermi–Dirac distribution, and T the temperature of the sample. The derivative of n_s with respect to the Fermi level is[28] $\frac{dn_s}{dE_F} = \frac{1}{k_B T}\frac{\epsilon}{qL^2}\frac{2m-1}{m^2}(1+C)$. The parameters m and C can be extracted from the shape of the measured current–voltage characteristic (Figure S5, Supporting Information). To reconstruct the density of trap states as a function of the energy, it is also necessary to relate the voltage, V, to the energy of the traps that are filled at this specific voltage. This can be done by extracting the activation energy E_A, defined as $E_A = -\frac{d\ln J}{d(k_B T)^{-1}}$, from the temperature-dependent SCLC curves at each voltage point. To extract the DOS_T, the expression for $\frac{dn_s}{dE_F}$ is deconvolved with respect to $\frac{df}{dE_F}$ (see Figure S6, Supporting Information).

After analyzing the data shown in Figure 3a and 3c we were able to extract the DOS_T as in **Figure 4** (code validation in Figure S7, Supporting Information). The analysis is consistent with previous reports: the total density of traps close to the valence band, obtained by integrating the lower part of the DOS_T with respect to energy, is confirmed to be close to $n_{tVB} \approx 3 \times 10^{10}$ cm^{-3}.[12] The same integration, performed in proximity of the conduction band region, leads to a value of $n_{tCB} \approx 3 \times 10^{11}$ cm^{-3}. The DOS_T appears to be localized in energy; a defined peak is observed at ≈0.2 eV from the conduction band, and at ≈0.1 eV from the valence band. These findings match DFT simulations that show the presence, in very small concentrations, of trap states close to the valence and conduction bands.[35]

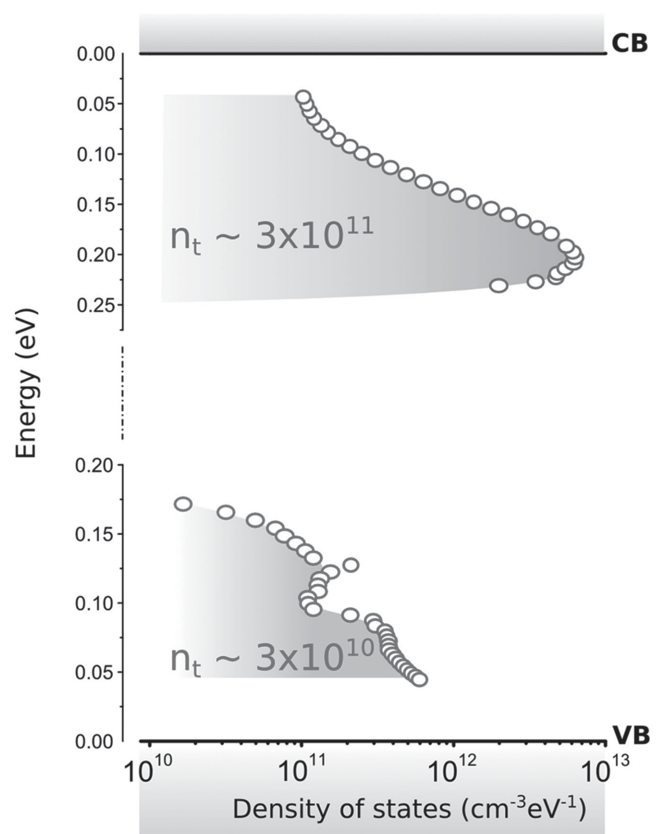

Figure 4. Density of the trap states within the bandgap so as extracted from the temperature-dependent SCLC method. Trap states are identified close to the conduction and the valence bands.

In conclusion, we carried out an in-depth electronic characterization of $MAPbI_3$ perovskite single crystals. We experimentally confirmed a series of important hypotheses advanced in previous theoretical studies. Furthermore, the crystals show high mobility and impressive diffusion lengths for both electrons and holes, confirming the ambipolar nature of these semiconductors.

Experimental Section

Crystal Synthesis: A mixture of PbI_2 (9.22 g, 0.02 mol) and CH_3NH_3I (9.54 g, 0.06 mol) was dissolved in 40 mL of gamma-butyrolactone (GBL) to form the solution. Dichloromethane (DCM) was used as the antisolvent.

Absorbance Measurements: The absorbance measurements were performed using a Jasco V-670 spectrophotometer. The sample was reduced to powder and the absorption was measured, based on the diffused reflectance, according to the established Kubelka–Munk method.

XRD Measurements: XRD data were collected from $MAPbI_3$ single-crystal powder using a Siemens D5000 Bragg-Brentano diffractometer.

UPS and XPS Measurements: UPS and XPS measurements were performed in a PHI 5500 Multi-Technique system with a base pressure of ≈10^{-9} Torr. The Fermi energy was calibrated to 0 eV. The sample was set to a take-off angle of 88° and a bias of −15 V was employed to collect

© 2016 WILEY-VCH Verlag GmbH & Co. KGaA, Weinheim

low-kinetic energy electrons efficiently. For XPS, monochromated Al Kα ($h\nu$ = 1486.7 eV) was used, and for UPS, nonmonochromated He Iα ($h\nu$ = 21.22 eV) was used. To measure the VBM relative to the Fermi level, the onset of the valence band was linearly extrapolated to the noise level.

Kelvin Probe Measurements: Kelvin probe measurements were obtained using a KPTechnology KP020 system. Both gold and aluminum were used as standard references.

I–V Measurements: Electrical contacts were defined on parallel facets of $MAPbBr_3$ single crystals using thermal evaporation of MoO_3/Au/Ag and e-beam evaporation of Ti for the hole-injecting and electron-injecting devices respectively. The thermal evaporator was kept in a N_2 filled glove box and was operated at pressures below 10^{-6} Torr. Immediately before the contact deposition the crystal surfaces were cleaned using dimethylformamide. The current–voltage measurements were performed using a Keithley 2400 sourcemeter. The temperature was controlled using an Advanced Research Systems DE 202 cryostat. The samples were kept in the dark during the measurement.

Acknowledgements

The authors thank Prof. Gennaro (Rino) Conte for the valuable discussions. This publication is based in part on the work supported by Award KUS-11-009-21 made by King Abdullah University of Science and Technology (KAUST), the Ontario Research Fund—Research Excellence Program, and the Natural Sciences and Engineering Research Council (NSERC) of Canada.

Received: October 19, 2015
Revised: January 26, 2016
Published online: March 2, 2016

[1] W. Yin, J. Yang, J. Kang, Y. Yan, S.-H. Wei, *J. Mater. Chem. A* **2014**, *3*, 8926.
[2] O. Malinkiewicz, A. Yella, Y. H. Lee, G. M. Espallargas, M. Grätzel, M. K. Nazeeruddin, H. J. Bolink, *Nat. Photonics* **2013**, *8*, 128.
[3] D. Liu, T. L. Kelly, *Nat. Photonics* **2013**, *8*, 133.
[4] M. Liu, M. B. Johnston, H. J. Snaith, *Nature* **2013**, *501*, 395.
[5] M. A. Green, K. Emery, Y. Hishikawa, W. Warta, E. D. Dunlop, *Prog. Photovoltaics Res. Appl.* **2015**, *23*, 1.
[6] W. S. Yang, J. H. Noh, N. J. Jeon, Y. C. Kim, S. Ryu, J. Seo, S. I. Seok, *Science* **2015**, *348*, 1234.
[7] A. Marchioro, J. Teuscher, D. Friedrich, M. Kunst, R. van de Krol, T. Moehl, M. Grätzel, J.-E. Moser, *Nat. Photonics* **2014**, *8*, 250.
[8] G. Giorgi, J.-I. Fujisawa, H. Segawa, K. Yamashita, *J. Phys. Chem. Lett.* **2013**, *4*, 4213.
[9] J. Kim, S.-H. Lee, J. H. Lee, K.-H. Hong, *J. Phys. Chem. Lett.* **2014**, *5*, 1312.
[10] J. Even, L. Pedesseau, J.-M. Jancu, C. Katan, *J. Phys. Chem. Lett.* **2013**, *4*, 2999.
[11] J. M. Azpiroz, E. Mosconi, J. Bisquert, F. De Angelis, *Energy Environ. Sci.* **2015**, *8*, 2118.
[12] D. Shi, V. Adinolfi, R. Comin, M. Yuan, E. Alarousu, A. Buin, Y. Chen, S. Hoogland, A. Rothenberger, K. Katsiev, Y. Losovyj, X. Zhang, P. A. Dowben, O. F. Mohammed, E. H. Sargent, O. M. Bakr, *Science* **2015**, *347*, 519.
[13] D. J. Dixon, K. P. Johnston, *AIChE J.* **1991**, *37*, 1441.
[14] H.-S. Kim, C.-R. Lee, J.-H. Im, K.-B. Lee, T. Moehl, A. Marchioro, S.-J. Moon, R. Humphry-Baker, J.-H. Yum, J. E. Moser, M. Grätzel, N.-G. Park, *Sci. Rep.* **2012**, *2*, 591.
[15] M. I. Saidaminov, A. L. Abdelhady, B. Murali, E. Alarousu, V. M. Burlakov, W. Peng, I. Dursun, L. Wang, Y. He, G. Maculan, A. Goriely, T. Wu, O. F. Mohammed, O. M. Bakr, *Nat. Commun.* **2015**, *6*, 7586.
[16] Q. Dong, Y. Fang, Y. Shao, P. Mulligan, J. Qiu, L. Cao, J. Huang, *Science* **2015**, *347*, 967.
[17] J. S. Kim, B. Lägel, E. Moons, N. Johansson, I. D. Baikie, W. R. Salaneck, R. H. Friend, F. Cacialli, *Synth. Met.* **2000**, *111–112*, 311.
[18] H. Baumgärtner, H. D. Liess, *Rev. Sci. Instrum.* **1988**, *59*, 802.
[19] A. Pfau, K. D. Schierbaum, *Surf. Sci.* **1994**, *321*, 71.
[20] P. Oelhafen, M. Liard, H.-J. Güntherodt, K. Berresheim, H. D. Polaschegg, *Solid State Commun.* **1979**, *30*, 641.
[21] L. Ley, R. A. Pollak, F. R. McFeely, S. P. Kowalczyk, D. A. Shirley, *Phys. Rev. B* **1974**, *9*, 600.
[22] Y. Fang, Q. Dong, Y. Shao, Y. Yuan, J. Huang, *Nat. Photonics* **2015**, *9*, 679.
[23] A. Rose, *Phys. Rev.* **1955**, *97*, 1538.
[24] P. Mark, W. Helfrich, *J. Appl. Phys.* **1962**, *33*, 205.
[25] M. M. Mandoc, F. B. Kooistra, J. C. Hummelen, B. de Boer, P. W. M. Blom, *Appl. Phys. Lett.* **2007**, *91*, 263505.
[26] M. Bailes, P. J. Cameron, K. Lobato, L. M. Peter, *J. Phys. Chem. B* **2005**, *109*, 15429.
[27] A. H. Ip, S. M. Thon, S. Hoogland, O. Voznyy, D. Zhitomirsky, R. Debnath, L. Levina, L. R. Rollny, G. H. Carey, A. Fischer, K. W. Kemp, I. J. Kramer, Z. Ning, A. J. Labelle, K. W. Chou, A. Amassian, E. H. Sargent, *Nat. Nanotechnol.* **2012**, *7*, 577.
[28] F. Schauer, R. Novotny, S. Nešpurek, *J. Appl. Phys.* **1997**, *81*, 1244.
[29] S. Nespurek, E. A. Silinsh, *Phys. Status Solidi* **1976**, *34*, 747.
[30] J. Dacuña, A. Salleo, *Phys. Rev. B: Condens. Matter Mater. Phys.* **2011**, *84*.
[31] C. Krellner, S. Haas, C. Goldmann, K. P. Pernstich, D. J. Gundlach, B. Batlogg, *Phys. Rev. B: Condens. Matter Mater. Phys.* **2007**, *75*.
[32] M. A. Lampert, A. Rose, R. W. Smith, *J. Phys. Chem. Solids* **1959**, *8*, 464.
[33] H. Lee, S. W. Cho, K. Han, P. E. Jeon, C.-N. Whang, K. Jeong, K. Cho, Y. Yi, *Appl. Phys. Lett.* **2008**, *93*, 043308.
[34] W.-J. Shin, J.-Y. Lee, J. C. Kim, T.-H. Yoon, T.-S. Kim, O.-K. Song, *Org. Electron.* **2008**, *9*, 333.
[35] A. Buin, P. Pietsch, J. Xu, O. Voznyy, A. H. Ip, R. Comin, E. H. Sargent, *Nano Lett.* **2014**, *14*, 6281.

© 2016 WILEY-VCH Verlag GmbH & Co. KGaA, Weinheim